Intrinsically Stable 2-GHz Polarization Modulation for Satellite-Based Quantum Key Distribution

Wenbin Luo, Yang Li, Yuhuai Li, Xueying Tao, Liying Han, Wenqi Cai, Juan Yin, Jigang Ren, Shengkai Liao, and Chengzhi Peng

***Abstract*—Satellite-based quantum key distribution (QKD) has made significant strides in the past few years, and an international space race toward practical quantum networks has begun. Being one major encoding method, highly robust, high-performance and miniaturized polarization modulation is critical to meet the needs of future satellite applications. Here, we employ the Sagnac-based method to realize inherent-stable polarization modulation and propose a novel optical design to achieve a state-of-the-art repetition rate of 2 GHz. This value approaches the theoretical repetition frequency limit with commercially-available phase modulators. Furthermore, the polarization encoder is miniaturized into a robust 6.0 cm × 6.5 cm module and two commercially mature phase modulators. A 90-min consecutive test was successfully performed, verifying the robustness of this scheme with an average quantum bit error rate as low as 0.42%. The presented intrinsically stable high-speed polarization modulation provides an effective solution for future satellite applications.**

***Index Terms*—Quantum key distribution, high-speed polarization modulation, Sagnac.**

I. Introduction

SINCE the first quantum key distribution (QKD) protocol proposed in 1984 [1], remarkable breakthroughs have been made in the past few decades, including fiber links [2], [3], [4], [5], [6], [7], [8], [9], free-space links [10], [11], [12], [13], [14], and even satellite-based links [15], [16], [17], [18], [19]. Recently, an international space race toward practical quantum networks has begun, and several proposals for satellites and quantum constellations have been reported [20], [21], [22], [23], [24], [25], [26]. Polarization encoding, due to the advantage of high fidelity and negligible loss in outer space, is widely applied in satellite-based QKD. For future satellite applications, the space-borne polarization encoder has to be highly robust to withstand the harsh environments during satellite launch and in-orbit operations, has to achieve high repetition frequency and low quantum bit error rate (QBER) to maximize the key generation rate, and has to be miniaturized to reduce the required volume and weight.

Thus far, several encoding schemes have been proposed [27], [28], [29], [30], [31], [32], [33], [34], [35], [36], [37], which can be generally classified into two categories. The first one is based on the balanced Mach–Zehnder (MZ) interferometer [37] or on the lithium niobate ($LiNbO_3$) phase modulator (PM) with the polarization-maintaining fiber (PMF) input aligned at 45° [28], [31], [32], [33]. Due to the two orthogonal light components transmitting in different MZ interferometer arms or different axes of the modulator, this polarization modulation is sensitive to external environmental disturbances. The requirement of strict working environments leads to complex structure thermal isolation and temperature control, resulting in large resource costs. This method also suffers from polarization mode dispersion (PMD), and additional compensation is required [31], [32], [33].

The other is based on interferometers that use either Sagnac loops [34], [35], [36] or Faraday mirrors [27], [30]. Because the typical time scale of the phase noise introduced by the transmission medium [38] is significantly longer than the propagation time (tens of nanoseconds) in the Sagnac interferometer, the phase difference between the two interferometer arms can be well canceled after transmission through the Sagnac loop. As a result, this method exhibits inherent robustness and can achieve long-term stability without any adjustment or compensation, which has been demonstrated in [34], [35], [36], [38]. Although remarkable achievements have been made in Sagnac-based polarization modulation [34], [35], [36], most of them are implemented by discrete modules with insufficient integration, while the repetition frequency can be further improved to approach the theoretical limit with commercially-available modulators.

In this paper, we have conducted, to the best of our knowledge, the first in-depth analysis of the repetition frequency limit of Sagnac-based polarization modulation. To overcome the electronics challenges when approaching the limit, we proposed a novel two-stage polarization modulation scheme through flexible optical design. Two sets of simplified binary electrical signals and two PMs are adopted to prepare the four polarization states utilized in the BB84 protocol. The proposed polarization encoder is composed of a customized 6.0 cm × 6.5 cm module

Manuscript received 10 August 2022; revised 18 September 2022; accepted 21 September 2022. Date of publication 26 September 2022; date of current version 4 October 2022. This work was supported in part by the National Key Research and Development Program of China under Grants 2020YFA0309701, 2020YFA0309703, and 2020YFE0200600, in part by the Shanghai Municipal Science and Technology Major Project under Grant 2019SHZDZX01, and in part by Anhui Provincial Natural Science Foundation under Grants 2008085MA29 and 2008085J03. *(Corresponding authors: Yang Li; Shengkai Liao.)*

The authors are with the Hefei National Research Center for Physical Sciences at the Microscale and School of Physical Sciences, University of Science and Technology of China, Hefei 230026, China, also with the Shanghai Research Center for Quantum Science and CAS Center for Excellence in Quantum Information and Quantum Physics, University of Science and Technology of China, Shanghai 201315, China, and also with the Hefei National Laboratory, University of Science and Technology of China, Hefei 230088, China (e-mail: wbluo@mail.ustc.edu.cn; liyang9@ustc.edu.cn; liyuhuai@ustc.edu.cn; taoxueying@ustc.edu.cn; hanly@mail.ustc.edu.cn; caiwq@ustc.edu.cn; yinjuan@ustc.edu.cn; jgren@ustc.edu.cn; skliao@ustc.edu.cn; pcz@ustc.edu.cn).

Digital Object Identifier 10.1109/JPHOT.2022.3209532

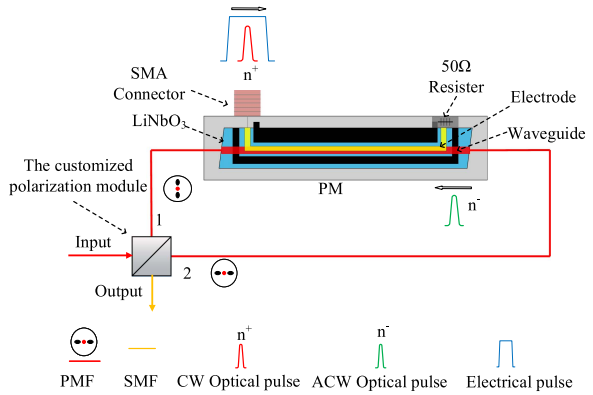

Fig. 1. Schematic of the typical polarization modulation based on a Sagnac interferometer. PMF, polarization-maintaining fiber; SMF, single-mode fiber; PM, phase modulator; SMA, SubMiniature version A; CW, clockwise; ACW, anti-clockwise.

and two commercially mature phase modulators, which are miniaturized and fit the demands of future satellite applications. We conducted a successful 90-min consecutive test at a repetition frequency of 2 GHz, which approached the repetition frequency limit with a commercially-available PM and was a state-of-the-art value for Sagnac-based polarization-encoding QKD systems.

This paper is organized as follows: in section 2, we analyze the repetition frequency limit of the Sagnac-based polarization modulation; in section 3, we introduce the proposed two-stage polarization modulation scheme; in section 4, we provide the experimental implementation and results; finally, we conclude and discuss in section 5.

II. Repetition Frequency Limit of Sagnac-Based Polarization Modulation

Schematic of the typical polarization modulation based on a Sagnac interferometer is presented in Fig. 1, consisting of a polarization module and a PM inside a Sagnac loop [35].

After entering the Sagnac interferometer, the incident optical pulses are divided into two portions, and both aligned to the slow axis of the polarization-maintaining fibers (PMFs). The vertically ($|H\rangle$) polarized portion travels in the clockwise (CW) direction, while the horizontally ($|V\rangle$) polarized portion travels in the anti-clockwise (ACW) direction. The PM is a commercially-available high-bandwidth traveling-wave $LiNbO_3$ phase modulator. The modulating electrical signal is input to the SMA (SubMiniature version A) connector and propagates clockwise in the strip electrode with a terminal load resistance of 50 Ω. When the optical pulses are transmitted in the PM waveguide, additional phases are applied to them by precisely matching the timing of the modulating electrical pulses and the optical pulses, resulting in the four polarization states ($|D\rangle$, $|A\rangle$, $|L\rangle$ and $|R\rangle$) in the BB84 protocol.

Ideally, the electrical pulses interact only with the CW optical pulses and are completely interleaved with the ACW. However, as the repetition frequency increases, the interaction between the electrical pulses and the ACW optical pulses is inevitable. An electrical pulse, while acting on a CW pulse, also interacts with

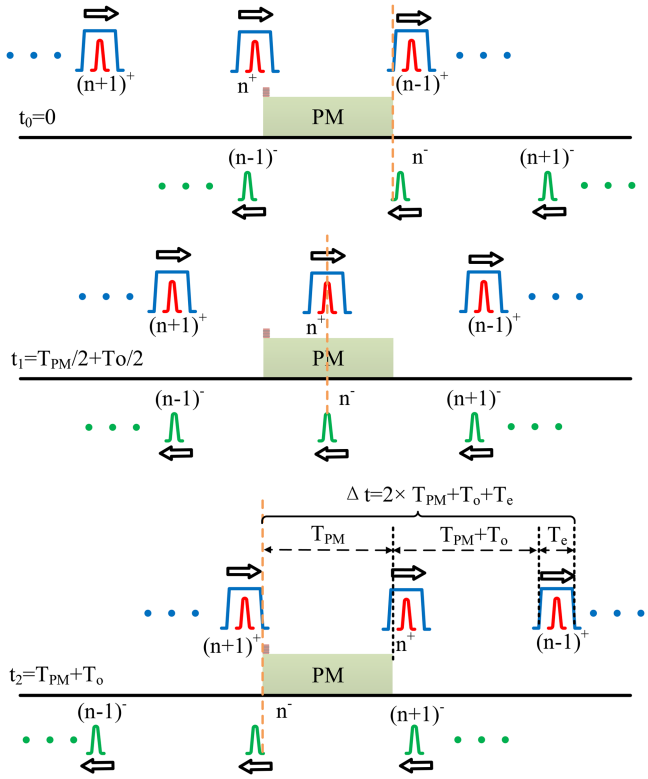

Fig. 2. Schematic of the repetition frequency limit of a Sagnac interferometer. For an electrical pulse, while acting on a CW pulse, it also interact with the corresponding ACW pulse.

the corresponding ACW pulse. When exiting the Sagnac loop, these two optical pulses will interfere with each other, and the phase modulation effect between them is partially neutralized, resulting in a decrease in the overall applied phase. As shown in Fig. 2, we assume that the ACW pulse n^- enters the PM at $t_0 = 0$, while the corresponding electrical pulse of the CW pulse $(n-1)^+$ exits the PM simultaneously. At $t_1 = T_{PM}/2 + T_o/2$ (T_{PM} represents the propagation time of the optical pulse along with the PM electrode and T_o refers to the duration of the optical pulse), the ACW pulse n^- propagates to the middle of the PM, and the electrical pulse acting on the CW pulse n^+ will also interact exactly with the ACW pulse n^- completely. At $t_2 = T_{PM} + T_o$, the ACW pulse n^- exits the PM completely, while the corresponding electrical pulse of the next CW pulse $(n+1)^+$ just enters the PM. The Δt in Fig. 2 is twice the minimum system repetition period. Therefore, the corresponding maximum repetition frequency is given by

$$f_{max} = \frac{2}{\Delta t} = \frac{1}{T_{PM} + \frac{T_o}{2} + \frac{T_e}{2}}, \tag{1}$$

where T_e refers to the duration of the electrical pulse, $T_{PM} = \frac{l_{PM}}{c/n_0}$ (l_{PM} refers to the PM length), c represents the speed of light in a vacuum, and n_0 is the refractive index of the PM waveguide. f_{max} is the intrinsic repetition frequency limit of the Sagnac loop, which is determined by T_{PM}, T_o, and T_e. Note that in order to obtain the maximum repetition rate, the loop delays of

the two arms inside the Sagnac must be finely controlled to be equal, within a tolerance of a few millimeters.

According to equation (1), considering a commercial $LiNbO_3$ PM with a length of 40 mm, a typical T_o of 70 ps and T_e of 220 ps, respectively, the theoretical repetition frequency limit f_{max} is 2.27 GHz. Limited by the length of the $LiNbO_3$ PM and the width of the modulated electrical signals, it is hardly to break through this repetition frequency limit with state-of-the-art commercial modulators. Besides, the previous works [34], [36] adopted the bidirectional configuration to prepare the polarization states. However, this scheme suffers a lower repetition frequency limit because the modulating electrical pulses must be wide enough to enable independent modulation of the reverse optical pulses.

III. Implementation of Two-Stage Polarization Modulation

For high-speed drive electronics, multi-amplitude signals are generally generated by the superposition of multi-channel signals [39]. The research in [35] adopted the single-stage scheme to realize the polarization modulation requires multi-stage electrical pulses to prepare the polarization states. However, generating a perfect multi-amplitude square wave signal to modulate light pulses is extremely challenging. Harsh electronic crosstalk and noise caused by the superposition of signals can degrade modulation performance and increase QBER. Moreover, as mentioned above, for Sagnac-based polarization modulation, the phase modulation effect will be partially neutralized when approaching the repetition frequency limit, which results in an equivalent half-wave voltage increase. This further increases the difficulty in achieving higher repetition rates.

To achieve modulation rate close to the limit, We have proposed a novel two-stage scheme, which consists of a customized polarization module and two Sagnac-based interferometers. We have completed the key technologies such as high polarization-maintaining fiber alignment and high-efficiency optical path coupling, and finally realized the integration of the polarization module. Schematic of the polarization modulation scheme is shown in Fig. 3(c). The polarization polarization process is as follows:

1) Linearly polarized optical pulses propagate along the slow axis of the input PMF. After being rotated by 45° and passing through a circulator (Cir1), the optical pulses are incident on port 1 of a polarization beam splitter (PBS1). The input polarization state can be expressed as

$$|\psi_0\rangle = \frac{1}{\sqrt{2}}(|H\rangle + |V\rangle). \tag{2}$$

2) The optical pulse is then divided into two portions by PBS1. The reflected (transmitted) portion is vertically (horizontally) polarized and is coupled into the slow axis of the PMF at port 2 (3). The portion then propagates along the first Sagnac interferometer (IF1) in the CW (ACW) direction. In the CW direction, the $LiNbO_3$ phase modulator introduces an additional phase φ_1 to the optical pulses by precisely matching the relative delay between the optical pulses and the driving electrical signals.

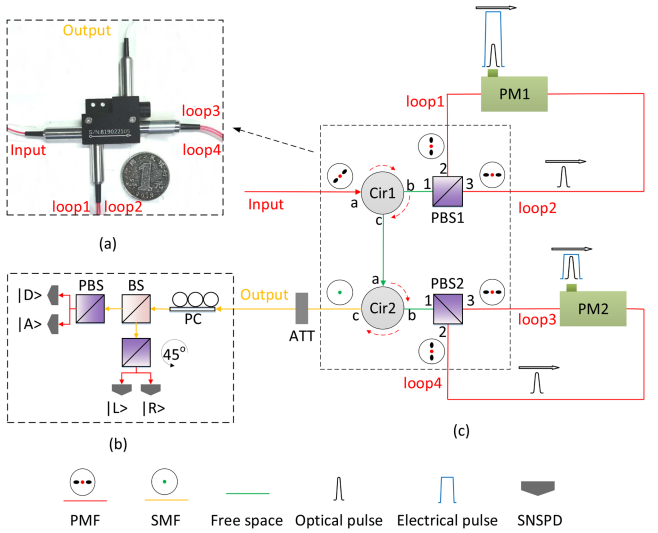

Fig. 3. (a) Photograph of the customized polarization module with a size of 6.0 cm × 6.5 cm. The insertion loss of the custom device is 6.56 dB. (b) Schematic of the polarization analysis module used to analyze the four generated polarization states for the BB84 protocol. (c) Schematic of the two-stage polarization modulation scheme. BS, beam splitter; PBS, polarization beam splitter; ATT, attenuator; PC, polarization controller; SNSPD, superconducting-nanowire single-photon detector. The fibers of the two arms inside the Sagnac are set to be of equal length.

Meanwhile, since both the CW and ACW portions travel along the slow axis of the PM fiber, no PMD is observed, and a single polarization mode propagates in the PM. After both portions pass through IF1, the polarization state can be expressed as

$$|\psi_1\rangle = \frac{1}{\sqrt{2}}\left(e^{i(\varphi_1+\delta_{c1})}|s\rangle_{c1} + e^{i\delta_{a1}}|s\rangle_{a1}\right), \tag{3}$$

where the subscripts $c1$ and $a1$ refer to the CW and ACW portions of IF1, respectively. Due to the Sagnac loop path, the common phases of δ_{c1} and δ_{a1} are applied to the two portions, respectively. Because the typical time scale of the phase noise introduced by the transmission medium [38] is significantly longer than the propagation time (tens of nanoseconds) in the Sagnac interferometer, the common phases of δ_{c1} and δ_{a1} can be considered equal on the Sagnac-loop time scale and can be omitted for the sake of simplicity.

3) The PMF between ports 2 and 3 of PBS1 helps achieve a 90° polarization rotation after the optical pulse passes through the IF1. The CW (ACW) portion output from the PMF at port 3 (2) reaches PBS1 again. After passing through Cir1 and Cir2, the CW (ACW) portion of IF1 is incident on port 1 of PBS2, totally transmitted (reflected) to port 3(2) due to its horizontal (vertical) polarization, and finally coupled into the slow axis of each PMF. After both portions pass through IF2, the polarization state can be expressed as

$$|\psi_2\rangle = \frac{1}{\sqrt{2}}\left(e^{i(\varphi_2+\delta_{c2})}|s\rangle_{c2} + e^{i\delta_{a2}}|s\rangle_{a2}\right), \tag{4}$$

where the subscripts $c2$ and $a2$ refer to the CW and ACW portions of IF2, respectively. Similar to the first stage, the common

phases of δ_{c2} and δ_{a2} can be considered equal on the Sagnac-loop time scale and can be omitted as well.

(4) The PMF between ports 2 and 3 of PBS2 helps achieve a 90° polarization rotation again after the optical pulse passes through IF2. The CW (ACW) portion finally remains in vertical (horizontal) polarization. Then the CW (ACW) portion of the IF2 output from the PMF at port 3 (2) reaches PBS2 and Cir2 again. The output polarization state can be written as

$$|\psi_3\rangle = \frac{1}{\sqrt{2}}\left(|H\rangle + e^{i(\varphi_2+\varphi_1)}|V\rangle\right). \quad (5)$$

By changing the additional phases of φ_1 and φ_2, a specific polarization state can be generated. For example, the output polarization state can be written as $|D\rangle = \frac{1}{\sqrt{2}}(|H\rangle + |V\rangle)$, $|L\rangle = \frac{1}{\sqrt{2}}(|H\rangle + i|V\rangle)$, $|A\rangle = \frac{1}{\sqrt{2}}(|H\rangle - |V\rangle)$, $|R\rangle = \frac{1}{\sqrt{2}}(|H\rangle - i|V\rangle)$, where ($\varphi_1$, φ_2) equals (0, 0), (0, $V_\pi/2$), (V_π, 0), and (V_π, $V_\pi/2$), respectively. By using the two sets of binary electrical signals, the four polarization states in the BB84 protocol can be realized.

The presented two-stage polarization modulation scheme inherits the robustness of the inherently stable Sagnac interferometer. Most importantly, this solution can simplify the demand of multiple-amplitude electrical signals and reduces electronic crosstalk, making it possible to approach the repetition frequency limit of the Sagnac loop.

IV. Experimental Demonstration and Results

We utilized a self-developed pulse generator board to produce the required binary electrical signals. A 1550-nm laser diode (LD) was driven by periodic electrical pulses to emit short optical pulses with a duration of ~70 ps. The output optical pulses were directly fed into the customized polarization module [Fig. 3(c)]. Two sets of electrical pulses with a duration of ~220 ps were adopted to drive the two PMs in the Sagnac interferometers and to apply the required additional phases. The raw half-wave voltage of the commercial $LiNbO_3$ PM we adopted is approximately 4.1 V. However, the measured equivalent half-wave voltage required in the experiment reached 6.5 V, due to the partial neutralization of the phase modulation effect when approaching the repetition frequency limit. After polarization modulation, the output optical signals were used for polarization analysis.

To prepare the four target polarization states for the BB84 protocol, pseudo-random binary electrical pulses with a repeated 1600-bit pattern were applied to the two PMs. The generated polarization states were attenuated to the single-photon level and analyzed using a polarization analysis module consisting of a PC for polarization compensation, a beam splitter, and two PBSs, as shown in Fig. 3(b). The output photons were then detected by four superconducting-nanowire single-photon detectors (SNSPDs). A time-correlated single-photon-counting (TCSPC) device (PicoQuant, HydraHarp 400) was utilized to analyze the measured results. The time bin width of the TCSPC device is set as 16 ps. The TCSPC device is time-synchronized by the electrical signal generated from the pulse generator board

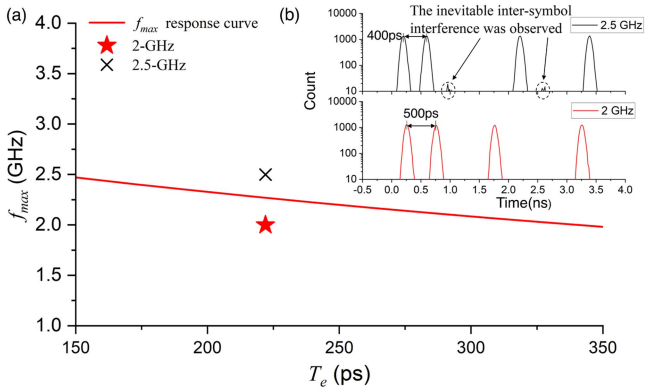

Fig. 4. (a) the theoretical repetition frequency limit f_{max} of a commercial $LiNbO_3$ PM under different T_e. The star represents the successfully achieved 2 GHz polarization modulation, close to the theoretical frequency limit. The cross represents the polarization modulation tested at 2.5 GHz. (b) The measured photon distributions of the polarization modulation tested at 2.5 GHz and 2 GHz. The inevitable inters-ymbol interference was observed between the adjacent pulses at 2.5 GHz.

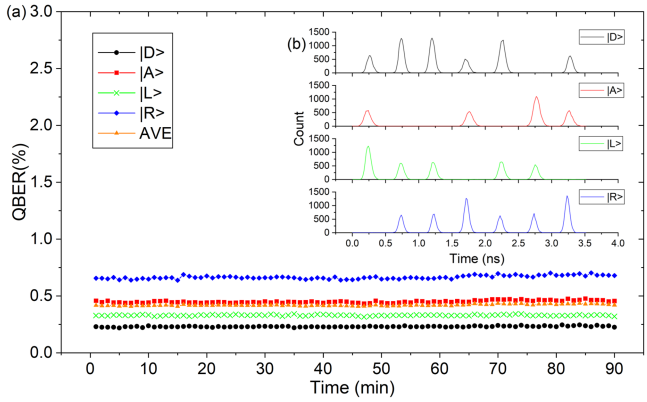

Fig. 5. (a) Measured average quantum bit error rates for 90 consecutive minutes. (b) Typically measured photon distributions of the four detectors ($|D\rangle$, $|A\rangle$, $|L\rangle$ and $|R\rangle$). The time interval between the adjacent two pulses is 500 ps, corresponding to a repetition frequency of 2 GHz.

and gives out the measured photon distributions after a count accumulation of 30 seconds.

For the adopted $LiNbO_3$ PM with a length of 40 mm, the corresponding f_{max} under different T_e is shown in Fig. 4(a). The rate of the pulse generator we adopted is 10 Gbps. The corresponding achievabe modulation frequencies are 2 GHz and 2.5 GHz, etc., and we have tested the performance of polarization modulation at these two repetition rates. The star in Fig. 4(a) represents the successfully achieved 2-GHz polarization modulation, close to the theoretical frequency limit. The cross represents the polarization modulation tested at 2.5 GHz, which has exceeded the frequency limit. An average QBER of $|D\rangle$ and $|A\rangle$ at 2.5 GHz reaches 0.71%, which is about twice the 0.35% at 2 GHz, and inevitable inter-symbol interference was observed between the adjacent pulses, as shown in Fig. 4(b).

Finally, a successful experimental test was conducted at a repetition frequency of 2 GHz. Typical photon distributions ($|D\rangle$, $|A\rangle$, $|L\rangle$, $|R\rangle$) are shown in Fig. 5(b). To demonstrate

the applicability of the presented two-stage polarization modulation scheme, a long-term polarization modulation test was conducted on an indoor optical platform without thermal isolation and temperature control. The relevant measured QBER results with a gate width of 176 ps are displayed in Fig. 5(a). The measured QBERs for the $|D\rangle$, $|A\rangle$, $|L\rangle$, $|R\rangle$ polarization states were $0.23 \pm 0.01\,\%$, $0.45 \pm 0.02\,\%$, $0.33 \pm 0.01\,\%$, and $0.67 \pm 0.03\,\%$, respectively. The average QBER of the four polarization states was $0.42 \pm 0.01\,\%$. The variation in the measured quantum bit error rate was as low as 0.03%, directly demonstrating the robustness of the presented modulation scheme. Compared with previous Sagnac implementations [29], [34], [35], [36], for the first time, the repetition frequency approached the repetition frequency limit of the Sagnac loop using commercial $LiNbO_3$ PMs.

V. Conclusion

In conclusion, we have analyzed the repetition frequency limit of the Sagnac-based polarization modulation and proposed a novel two-stage polarization modulation, which can approach this limit with commercially-available devices. Meanwhile, it inherits the robustness of the inherently stable Sagnac interferometer, thus exhibiting the advantages of being free from PMD and being insensitive to environmental influences. Finally, we conducted a 90-min experimental demonstration at a repetition frequency of 2 GHz to demonstrate the robustness of the presented scheme. The proposed polarization encoder is composed of a miniaturized 6.0 cm $\times$ 6.5 cm module and two commercial phase modulators. Therefore, the presented intrinsically stable high-speed polarization modulation can be widely applied to satellite applications.

Combined with Sagnac-based intensity modulation [40], an intrinsically stable light source for decoy-state BB84 quantum key distribution can be realized. The idea of adopting two Sagnac-based interferometers can simplify the demand of multiple-amplitude electrical signals, making it technically feasible to approach the repetition frequency limit, at the additional cost of an interferometer and a PM. This cost, relative to its performance improvement, is affordable. The follow-up works focus on two aspects, including the development of an integrated light source and the validation tests of space environments (mechanical vibration, thermal vacuum environment, space radiation, etc.), to further verify its inherent stability and lay the foundation for future satellite payloads.

There is still room for improvement in the repetition frequency of Sagnac-based polarization modulation. As shown in equation (1), the repetition frequency limit mainly depends on T_{PM}, T_e and T_o, and the main bottleneck is the PM waveguide and electrode length. In order to increase this limit, PM with reduced waveguide length or integrated $LiNbO_3$ electro-optic modulators [41], [42] can be adopted. For example, for an integrated $LiNbO_3$ modulator with a length of 5 mm [41], T_{PM} can be estimated to be 36 ps. A T_e of 80 ps and T_o of 40 ps are also feasible with improved electronics and high-speed LD. The corresponding f_{max} is approximately 10 GHz. This can be attempted in the subsequent researches.

References

[1] C. H. Bennett and G. Brassard, "Quantum cryptography: Public key distribution and coin tossing," in *Proc. Int. Conf. Comput. Syst. Signal Process.*, 1984, pp. 175–179.

[2] A. Muller, J. Breguet, and N. Gisin, "Experimental demonstration of quantum cryptography using polarized photons in optical fibre over more than 1 km," *Europhysics Lett.*, vol. 23, no. 6, pp. 383–388, Aug. 1993.

[3] C. Z. Peng et al., "Experimental long-distance decoy-state quantum key distribution based on polarization encoding," *Phys. Rev. Lett.*, vol. 98, no. 1, 2007, Art. no. 010505.

[4] D. Rosenberg et al., "Long-distance decoy-state quantum key distribution in optical fiber," *Phys. Rev. Lett.*, vol. 98, no. 1, 2007, Art. no. 010503.

[5] Y. Liu et al., "Decoy-state quantum key distribution with polarized photons over 200 km," *Opt. Exp.*, vol. 18, no. 8, Apr. 2010, Art. no. 8587.

[6] B. Korzh et al., "Provably secure and practical quantum key distribution over 307 km of optical fibre," *Nature Photon.*, vol. 9, no. 3, pp. 163–168, 2015.

[7] A. Boaron et al., "Secure quantum key distribution over 421 km of optical fiber," *Phys. Rev. Lett.*, vol. 121, no. 19, Nov. 2018, Art. no. 190502.

[8] S. Wang et al., "Twin-field quantum key distribution over 830-km fibre," *Nature Photon.*, vol. 16, no. 2, pp. 154–161, 2022.

[9] J. P. Chen et al., "Quantum key distribution over 658 km fiber with distributed vibration sensing," *Phys. Rev. Lett.*, vol. 128, no. 18, 2022, Art. no. 180502.

[10] C. H. Bennett and G. Brassard, "Experimental quantum cryptography: The dawn of a new era for quantum cryptography: The experimental prototype is working," *ACM SIGACT News*, vol. 20, no. 4, pp. 78–80, Nov. 1989.

[11] W. T. Buttler et al., "Practical free-space quantum key distribution over 1 km," *Phys. Rev. Lett.*, vol. 81, no. 15, pp. 3283–3286, 1998.

[12] R. J. Hughes, J. E. Nordholt, D. Derkacs, and C. G. Peterson, "Practical free-space quantum key distribution over 10 km in daylight and at night," *New J. Phys.*, vol. 4, pp. 43–1, Jul. 2002.

[13] T. Schmitt-Manderbach et al., "Experimental demonstration of free-space decoy-state quantum key distribution over 144 km," *Phys. Rev. Lett.*, vol. 98, no. 1, 2007, Art. no. 010504.

[14] S. K. Liao et al., "Long-distance free-space quantum key distribution in daylight towards inter-satellite communication," *Nature Photon.*, vol. 11, no. 8, pp. 509–513, 2017.

[15] S. K. Liao et al., "Satellite-to-ground quantum key distribution," *Nature*, vol. 549, no. 7670, pp. 43–47, Aug. 2017.

[16] S. K. Liao et al., "Space-to-ground quantum key distribution using a small-sized payload on Tiangong-2 space lab," *Chin. Phys. Lett.*, vol. 34, no. 9, Aug. 2017, Art. no. 090302.

[17] S. K. Liao et al., "Satellite-relayed intercontinental quantum network," *Phys. Rev. Lett.*, vol. 120, no. 3, Jan. 2018, Art. no. 030501.

[18] A. Villar et al., "Entanglement demonstration on board a nano-satellite," *Optica*, vol. 7, no. 7, pp. 734–737, 2020.

[19] Y. A. Chen et al., "An integrated space-to-ground quantum communication network over 4,600 kilometres," *Nature*, vol. 589, no. 7841, pp. 214–219, Jan. 2021.

[20] D. K. Oi et al., "Cubesat quantum communications mission," *EPJ Quantum Technol.*, vol. 4, pp. 1–20, 2017.

[21] S. P. Neumann et al., "Q3sat: quantum communications uplink to a 3 u cubesat–feasibility & design," *EPJ Quantum Technol.*, vol. 5, pp. 1–24, 2018.

[22] H. Podmore et al., "Optical terminal for Canada's quantum encryption and science satellite (qeyssat)," in *Proc. IEEE Int. Conf. Space Opt. Syst. Appl.*, 2019, pp. 1–5.

[23] R. Haber, D. Garbe, K. Schilling, and W. Rosenfeld, "Qube-a cubesat for quantum key distribution experiments," in *Proc. Adv. Technol. I., AIAA/USU Conf. Small Satellites, SSC18-III-05*, 2018, pp. 1–8.

[24] E. Kerstel, A. Gardelein, M. Barthelemy, M. Fink, S. K. Joshi, and R. Ursin, "Nanobob: A cubesat mission concept for quantum communication experiments in an uplink configuration," *EPJ Quantum Technol.*, vol. 5, no. 1, pp. 1–30, 2018.

[25] C. Dalibot and S. Tustain, "The preliminary thermal design for the speqtre cubesat," in *Proc. Int. Conf. Environ. Syst.*, 2020. [Online]. Available: http://hdl.handle.net/2346/86436

[26] L. Mazzarella et al., "Quarc: Quantum research cubesat–a constellation for quantum communication," *Cryptography*, vol. 4, no. 1, p. 7, 2020.

[27] I. Lucio-Martinez, P. Chan, X. Mo, S. Hosier, and W. Tittel, "Proof-of-concept of real-world quantum key distribution with quantum frames," *New J. Phys.*, vol. 11, no. 9, Sep. 2009, Art. no. 095001.

[28] M. Jofre et al., "100 MHz amplitude and polarization modulated optical source for free-space quantum key distribution at 850 nm," *J. Lightw. Technol.*, vol. 28, no. 17, pp. 2572–2578, Sep. 2010.
[29] S. Li, H. Q. Ma, L. A. Wu, and G. J. Zhai, "High-speed polarization controller for all-fiber quantum communication systems," *Acta Phys. Sin.*, vol. 62, no. 8, pp. 1–5, 2013.
[30] J. Wang et al., "Experimental demonstration of polarization encoding quantum key distribution system based on intrinsically stable polarization-modulated units," *Opt. Exp.*, vol. 24, no. 8, 2016, Art. no. 8302.
[31] A. Duplinskiy, V. Ustimchik, A. Kanapin, V. Kurochkin, and Y. Kurochkin, "Low loss QKD optical scheme for fast polarization encoding," *Opt. Exp.*, vol. 25, no. 23, Nov. 2017, Art. no. 28886.
[32] F. Grünenfelder, A. Boaron, D. Rusca, A. Martin, and H. Zbinden, "Simple and high-speed polarization-based QKD," *Appl. Phys. Lett.*, vol. 112, no. 5, Jan. 2018, Art. no. 051108.
[33] F. Grünenfelder, A. Boaron, D. Rusca, A. Martin, and H. Zbinden, "Performance and security of 5 GHz repetition rate polarization-based quantum key distribution," *Appl. Phys. Lett.*, vol. 117, no. 14, 2020, Art. no. 144003.
[34] C. Agnesi, M. Avesani, A. Stanco, P. Villoresi, and G. Vallone, "All-fiber self-compensating polarization encoder for quantum key distribution," *Opt. Lett.*, vol. 44, no. 10, May 2019, Art. no. 2398.
[35] Y. Li et al., "High-speed robust polarization modulation for quantum key distribution," *Opt. Lett.*, vol. 44, no. 21, Nov. 2019, Art. no. 5262.
[36] M. Avesani, C. Agnesi, A. Stanco, G. Vallone, and P. Villoresi, "Stable, low-error, and calibration-free polarization encoder for free-space quantum communication," *Opt. Lett.*, vol. 45, no. 17, pp. 4706–4709, Sep. 2020. [Online]. Available: http://ol.osa.org/abstract.cfm?URI=ol-45-17-4706
[37] Z. Yan et al., "Novel high-speed polarization source for decoy-state BB84 quantum key distribution over free space and satellite links," *J. Lightw. Technol.*, vol. 31, no. 9, pp. 1399–1408, 2013.
[38] J. Minář, H. De Riedmatten, C. Simon, H. Zbinden, and N. Gisin, "Phase-noise measurements in long-fiber interferometers for quantum-repeater applications," *Phys. Rev. A*, vol. 77, no. 5, 2008, Art. no. 052325.
[39] X. Liu, M.-Q. Huang, H. Min, G. Jin, X. Jiang, and C.-Z. Peng, "A 5 GHz and 7.5 v multi-amplitude modulator driving circuit for practical high-speed quantum key distribution," *Rev. Sci. Instrum.*, vol. 91, no. 2, 2020, Art. no. 024705.
[40] G. L. Roberts et al., "Patterning-effect mitigating intensity modulator for secure decoy-state quantum key distribution," *Opt. Lett.*, vol. 43, no. 20, Oct. 2018, Art. no. 5110.
[41] C. Wang et al., "Integrated lithium niobate electro-optic modulators operating at CMOS-compatible voltages," *Nature*, vol. 562, no. 7725, pp. 101–104, 2018.
[42] M. He et al., "High-performance hybrid silicon and lithium niobate Mach–Zehnder modulators for 100 Gbit s- 1 and beyond," *Nature Photon.*, vol. 13, no. 5, pp. 359–364, 2019.